Calculation of electromagnetic properties of regular and random arrays of metallic and dielectric cylinders

R. C. McPhedran,[1] L. C. Botten,[2] A. A. Asatryan,[1] N. A. Nicorovici,[1] P. A. Robinson,[1] and C. M. de Sterke[1]
[1]*School of Physics, University of Sydney, NSW 2006, Australia*
[2]*School of Mathematical Sciences, University of Technology, Sydney, P.O. Box 123, Broadway, NSW 2007, Australia*
(Received 4 June 1999)

A method is developed to calculate electromagnetic properties of arrays of metallic and dielectric cylinders. It incorporates and exploits cylindrical boundary conditions and Rayleigh identities for efficient, high-accuracy calculation of scattering off individual layers that are stacked into arrays using scattering matrices. The method enables absorption, dispersion, and randomness to be incorporated efficiently, and reproduces known results with vastly improved speed and accuracy. It is used to demonstrate existence of states introduced into photonic band gaps of a dielectric array by disorder, and anomalous absorption behavior in arrays of aluminum cylinders. [S1063-651X(99)01511-1]

PACS number(s): 03.50.De, 42.25.Bs, 78.20.Bh, 78.20.Ci

We present an efficient, high-accuracy method to calculate the electromagnetic properties of regular or random arrays of cylinders in a stratified background. The optical properties of such arrays, regular or random, are being studied for application to novel photonic devices and band-gap materials, with the aim of controlling the flow of light. Materials of this type are the optical analogs of semiconductors, and tailoring of their band structure, density of states, defects, and wave localization properties is a promising tool for the design of materials with specified optical properties [1,2].

Our method, which is constructed for geometries as in Fig. 1, has advantages of generality, accuracy, and speed. It can deal with any number of nonoverlapping cylinders in the unit cell of each layer, arranged arbitrarily. It uses local coordinates around each cylinder for easy and accurate imposition of boundary conditions at their surfaces, even when the refractive index contrast with the embedding medium is arbitrarily large. It achieves its speed by dealing with each layer as a separate problem, then coupling layers by a recurrence technique, avoiding the inversion of large matrices. It also allows one to use measured optical properties, so that idealized (e.g., Lorentz) models of the materials are not required. Though some elements of our technique are used elsewhere, it is unique in uniting and generalizing them in a single formulation. By contrast, plane-wave methods [3] suffer inaccuracy due to the Gibbs phenomenon when the index contrast is large, as in metallic systems, the transfer matrix method [4,5] suffers from instability and inaccuracy for structures with a moderate or large number of inclusions per unit cell, while finite-difference time-domain methods [6] require simple analytic forms for the material response.

The class of methods most closely related to ours is the Korringa-Kohn-Rostoker (KKR) type, which have been widely used to calculate electronic energy bands in solids, and which implicitly incorporate lattice sums in matrix elements. The closest relative, the layer KKR method of Stefanou *et al.* [7], was developed for spheres. However, this method uses the relatively slow Ewald summation technique to evaluate matrix elements, whereas we use rapid, accurate expressions for the global lattice sums due to Twersky [8]. We also use local lattice sums for each of the cylinders in the unit cell of each layer to improve accuracy and speed further. We note that of the over 20 articles in the photonic band gap bibliography [9] dealing with metallic photonic crystals, all use the Drude model rather than measured optical properties of real metals, as used here. Some recent work [10] does use measured properties, but deals with a single grating of cylinders, not a stack of gratings. Finally, although some other methods can deal with inclusions of arbitrary shape, subject to the inaccuracies mentioned above, they are most often applied to structures with cylindrical inclusions, the structure for which our method is optimized and one that allows the study of a wide range of physical phenomena.

We present results that highlight the key advantages of our method. The first concerns stacks of cylinders with random refractive indexes, for which our results are more accurate and of higher resolution than any presented before. This lets us identify strongly polarization dependent, disorder-induced features in the photonic band gap. We also consider a regular stack of aluminum cylinders, for which the use of measured optical properties leads to pronounced and surprising new absorption features.

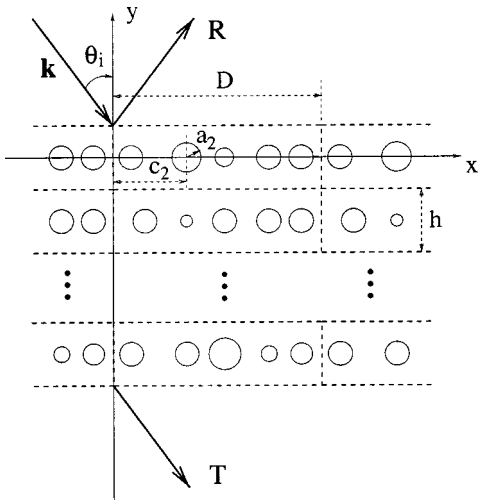

FIG. 1. Three layers of a grating stack are shown, together with the incident wave and the reflected and transmitted zeroth orders of diffraction from the stack.

 © 1999 The American Physical Society

We consider a plane wave of wavelength λ incident in free space at an angle θ_i on the structure in Fig. 1, in which each layer has a unit cell of N_c nonoverlapping cylinders, with radii a_l and refractive indexes n_l, located with centers on the midline with $x=c_l$. This cell is replicated with period D along the x axis; $d=D/N_c$ is the mean separation of cylinders. There are N_L layers in the full structure, with the separation h chosen to equal d for present purposes, although this is not essential. Note that a_l and n_l may vary between cylinders, and c_l may vary between layers. The only essential requirement is that a common period D can be identified for all layers. We solve the scattering problem using a method devised for normal incidence [11] and later generalized to arbitrary θ_i [8]. We generalize it to arbitrary N_c and N_L.

The fields around each cylinder are specified in terms of a single component ($V=E_z$ for TM polarization, $V=H_z$ for TE polarization, where z is the direction of the cylinder axes). The potential is specified in local polar coordinates (r_l,θ_l) via the Bessel expansion

$$V(r_l,\theta_l)=\sum_{m=-\infty}^{\infty}[A_m^l J_m(kr_l)+B_m^l Y_m(kr_l)]e^{im\theta_l}, \quad (1)$$

for $r_l>a_l$, with a similar expansion for $r_l<a_l$. These expansions are matched at $r_l=a_l$ using continuity of tangential field components. This enables the internal ($r_l<a_l$) coefficients to be eliminated, giving

$$A_m^l=-M_m^l B_m^l, \quad (2)$$

where the M_m^l depend on polarization, wave number k, and n_l [12]. The boundary conditions at the cylinders are thus satisfied for *any* complex n_l, without exhibiting the Gibbs phenomenon that plagues Fourier methods.

The coefficients B_m^l are found using a Rayleigh identity [13], according to which the first term in Eq. (1), corresponding to the source-free part of V, must have its sources on all cylinders except l, or at infinity. Hence,

$$\sum_{m=-\infty}^{\infty}A_m^l J_m(kr_l)e^{im\theta_l}=\exp[ik(x\sin\theta_i-y\cos\theta_i)]+\sum_{m=-\infty}^{\infty}\sum_{q\neq l}B_m^q Y_m(k|\mathbf{r}_l-\mathbf{r}_q|)e^{im\theta_{lq}}, \quad (3)$$

where θ_{lq} is the polar angle of $\mathbf{r}_l-\mathbf{r}_q$ and the sum over $q\neq l$ includes all cylinders but l in the central unit cell, and all cylinders in other cells. The Bloch condition and Graf's addition theorem [14] are used to give a set of linear equations for B_m^l:

$$\sum_{m=-\infty}^{\infty}S_{n-m}B_m^l+iM_n^l B_n^l+\sum_{q=1,q\neq l}^{N_c}\sum_{m=-\infty}^{\infty}S_{n-m}^{lq}B_m^q=-i(-1)^n\exp[ikc_l\sin\theta_i]\exp(in\theta_i). \quad (4)$$

Here the S_m^{lq} are lattice sums for the local environment of each cylinder, which are used to reduce the sums over cylinders in Eq. (4) to just those lying in the central unit cell. They can be obtained from global lattice sums S_m using Graf's addition theorem. The global sums are evaluated using methods described previously [8,13].

For given θ_i, Eq. (4) is solved for the B_m^l, from which the coefficients of outgoing plane waves $\exp[i(\alpha_p x+\chi_p y)]$ from the given layer are determined: R_p in the $+y$ (reflection) direction and T_p in the $-y$ (transmission) direction. Here $\chi_p=(k^2-\alpha_p^2)^{1/2}$, with

$$\alpha_p=k\sin\theta_p=k\sin\theta_i+2\pi p/D, \quad (5)$$

$$R_p=\frac{1}{iD\chi_p}\sum_{m=-\infty}^{\infty}\sum_{l=1}^{N_c}B_m^l e^{-i(m\theta_p+\alpha_p c_l)}, \quad (6)$$

and similarly for T_p. The amplitudes R_p and T_p constitute one column of the scattering matrices ρ and τ, respectively; the full matrices follow by varying θ_i over the angles θ_p of the diffraction orders of the layer. They contain the data needed from one layer in order to solve a stack. In our calculations we take $|p|\leq P$ and $|m|\leq M$, so $N_M=2M+1$ is the number of cylindrical harmonics used and $N_P=2P+1$ is the order of the scattering matrices used to couple the layers.

If reflection ρ_j and transmission τ_j matrices for layers $j=1$ to N are known, the reflection $\mathcal{R}$ and transmission $\mathcal{T}$ matrices with layer $N+1$ added are

$$\mathcal{R}_{N+1}=\rho_{N+1}+\tau_{N+1}\mathcal{R}_N(\mathcal{I}-\rho_{N+1}\mathcal{R}_N)^{-1}\tau_{N+1}, \quad (7)$$

$$\mathcal{T}_{N+1}=\mathcal{T}_N(\mathcal{I}-\rho_{N+1}\mathcal{R}_N)^{-1}\tau_{N+1}, \quad (8)$$

where $\mathcal{I}$ is the identity matrix of order N_P. We thus recursively find the complex reflection and transmission coefficients of a stack with an arbitrary number N_L of layers. Further details will be given elsewhere [15].

Accuracy was verified by comparing the results for a regular array of dielectric cylinders with those of Bell *et al.* [5], a layer of aluminum cylinders with those of Horwitz *et al.* [16], and transmission of multiple layers of perfectly conducting cylinders with band structures for square and hexagonal arrays [17]. We also checked reciprocity and energy conservation, which are satisfied to machine precision, independent of truncation to finite N_M and N_P, even for absorbing cylinders.

Parameters N_M and N_P are determined by λ, the n_l, and the minimum distance between cylinders; N_M is set by convergence for a single layer, N_P by that for the stack. At long wavelengths we obtain accurate results with $N_P=3$ or 5, and N_P increases as λ and h decrease. For short wavelengths $N_M\sim a/\lambda$, while at very long wavelengths accurate results are obtained using $N_M=3$ and $N_P=1$, with the scattering matrices reducing to scalars. For large systems the runtime scales as $N_L\max\{(N_M N_c)^3,N_P^3\}$, the first term in the brackets is due to matrix inversions for a single layer, and the second arising from inversions needed for layer coupling. The linear dependence on N_L means we can treat systems with large N_L much more efficiently than direct inversion, nonlayer methods [18], which scale as N_L^3.

Below we consider periodic square arrays of cylinders of identical radius in free space. In Figs. 2 and 3, we consider a stack of ten layers of dielectric cylinders, with $N_c=5$, refractive indexes uniformly distributed between 2.8 and 3.2, $a=0.3d$, and $D=5d$. The solid line in Fig. 2 shows transmit-

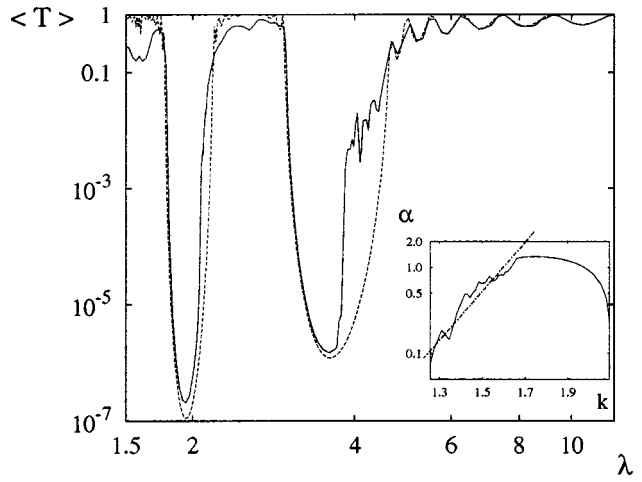

FIG. 2. Transmittance averaged over 100 realizations vs wavelength for a random dielectric array with parameters given in the text. Inset: intensity attenuation coefficient α vs k. The dot-dash line highlights the Urbach tail.

tance vs wavelength for TM polarization, averaged over 100 realizations per wavelength. For $\lambda \approx 0.3D = 1.5d$, $N_M = 21$, and $N_P = 27$ yielded transmittances accurate to five decimal places, taking around 40 s per wavelength per realization on a 500 Mflop processor. For $\lambda \approx 20D = 100d$, $N_M = 9$, and $N_P = 1$ sufficed, taking around 5 s per wavelength per realization.

In Fig. 2 we also compare the transmittance of the randomized stack with that of its periodic counterpart (dashed line). The transmittance is not strongly affected by disorder except at the long wavelength sides of the two band gaps, causing them to narrow. Note the fine structure in the first gap and the exponential behavior of the attenuation coefficient α vs k evident in the inset to Fig. 2. Here, $\alpha = -\langle \ln T \rangle / N_L h$, where T is the total energy transmitted in all propagating orders and $\langle \cdots \rangle$ denotes ensemble averaging. This shows formation of an Urbach-like tail, the extension of the spectrum of states into the gap by disorder, as in analogous semiconductor systems [19]. The asymmetry in the effects of disorder on the band gaps indicates that states on the low-frequency side of the gap are more affected by index disorder than the high-frequency ones [2]. Figure 2 should be

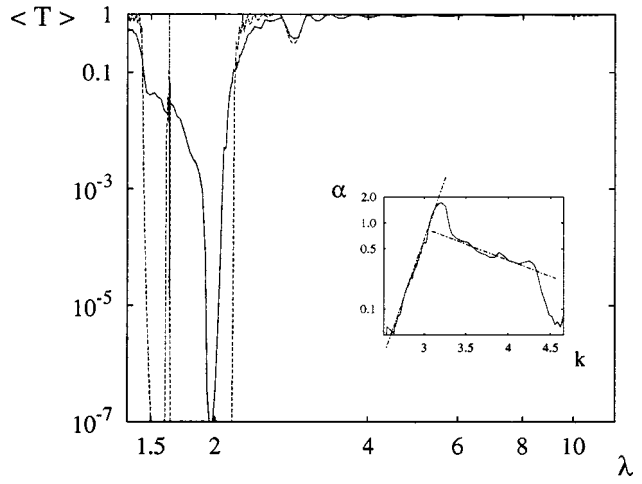

FIG. 3. As for Fig. 2, but for TE polarization.

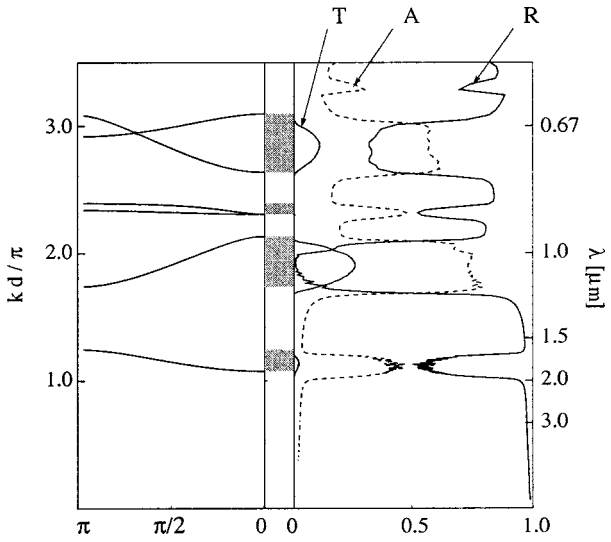

FIG. 4. Left panel: photonic band diagram for TM polarization ($V = E_z$) for a square array of perfectly conducting cylinders, with parameters given in the text and **k** along the Γ-X axis shown in the inset; the horizontal axis gives values of $k \sin \theta_i$. Right panel: reflectance R, transmittance T, and absorptance A for 25 layers of aluminum cylinders. Shaded bars between the panels denote bands.

compared with Fig. 4 of Sigalas *et al.* [20], obtained using a transfer-matrix method [4] whose results were less accurate ($\pm 20\%$) and did not have the resolution to exhibit the physically significant features evident here.

Figure 3 is similar to Fig. 2 but is for wavelengths in TE polarization. The first band gap is weak, so the effects of disorder are clearest in the prominent second gap, which is strongly narrowed, with states entering from both sides. The inset shows two Urbach tails regions with different slopes; TE polarization thus shows asymmetry similar to TM polarization (Fig. 2). The periodic structure has a narrow band around $\lambda = 1.63d$, which is almost eliminated by disorder.

The right side of Fig. 4 shows reflectance, transmittance, and absorption vs wave number at $\theta_i = 0$ for a periodic square stack of 25 layers of aluminum cylinders, with $d = 1$ μm, $a = 0.2$ μm, and complex refractive index from standard tables [21]. The number of layers is chosen so the stack's long wavelength transmittance is negligible. Note the strong absorption by the array, even where the reflectance of solid aluminum is over 98%. The left side of Fig. 4 shows the photonic band structure for a square array of perfectly conducting cylinders: absorptance peaks at right correspond to the photonic bands at left. As a varies, the bands in Fig. 4 move, with the position of the lowest scaling as $\lambda^2 \propto \ln(d/2a)$ [17,22]. Thus, as a decreases, the absorption peak moves to longer wavelengths and widens. Hence, remarkably, as $a \to 0$ the enhanced absorption shifts further into the region where bulk aluminum strongly reflects. The curves in the right panel of Fig. 4 correspond to a single angle of incidence (the vertical line through Γ) in the left panel. The fact that these curves are sensitive to the full band Γ-X is due to the infinite number of grating orders p in Eq. (5), which sample this whole interval.

In summary, we have developed a method of calculating electromagnetic properties of regular or random arrays of

cylinders, which can provide results of unprecedented accuracy and resolution for a wide variety of problems, using workstations rather than supercomputers. Already, this method has revealed the existence of Urbach tails of states introduced into photonic band gaps by disorder, and anomalous absorption behavior in arrays of metal cylinders. We will pursue further applications to dispersive and lossy photonic crystals, and to the study of localization in two-dimensional disordered systems.

We thank D.R. McKenzie for helpful suggestions. The Australian Research Council supported this work.

[1] C. M. Soukoulis, *Photonic Band Gaps and Localization* (Plenum, New York, 1993).
[2] J. D. Joanopoulos, R. D. Meade, and J. N. Winn, *Photonic Crystals: Molding the Flow of Light* (Princeton University, Princeton, NJ, 1995).
[3] K. M. Leung and Y. F. Liu, Phys. Rev. Lett. **65**, 2646 (1990).
[4] J. B. Pendry and A. MacKinnon, Phys. Rev. Lett. **69**, 2772 (1992).
[5] P. M. Bell, J. B. Pendry, L. Martin Moreno, and A. J. Ward, Comput. Phys. Commun. **85**, 306 (1995).
[6] C. T. Chan *et al.*, Physica A **211**, 411 (1994).
[7] N. Stefanou, V. Karathonos, and A. Modinos, J. Phys.: Condens. Matter **4**, 7389 (1992).
[8] V. Twersky, Arch. Ration. Mech. Anal. **8**, 323 (1961).
[9] J. Dowling, H. Everitt, and E. Yablonovitch, URL http://home.earthlink.net/~jpdowling/pbgbib.html
[10] F. J. García-Vidal, J. M. Pitarke, and J. B. Pendry, Phys. Rev. B **58**, 6783 (1998).
[11] W. von Ignatowsky, Ann. Phys. (Leipzig) **44**, 369 (1914).
[12] R. C. McPhedran, N. A. Nicorovici, and L. C. Botten, J. Electromagn. Waves Appl. **11**, 981 (1997).
[13] R. C. McPhedran, N. A. Nicorovici, L. C. Botten, and Bao Ke-Da, in *IMA Volumes in Mathematics and its Applications*, edited by G. Papanicolau (Springer-Verlag, New York, 1997), Vol. 96, p. 155.
[14] F. W. J. Olver, in *Handbook of Mathematical Functions*, edited by M. Abramowitz and I. A. Stegun (Dover, New York, 1972), p. 363.
[15] R. C. McPhedran *et al.*, Aust. J. Phys. **52**, 791 (1999).
[16] C. M. Horwitz, R. C. McPhedran, and J. Beunen, J. Opt. Soc. Am. **68**, 1023 (1978).
[17] N. A. Nicorovici, R. C. McPhedran, and L. C. Botten, Phys. Rev. E **52**, 1135 (1995).
[18] D. Felbacq, G. Tayeb, and D. Maystre, J. Opt. Soc. Am. A **11**, 2526 (1994).
[19] F. Urbach, Phys. Rev. **92**, 1324 (1953).
[20] M. M. Sigalas, C. M. Soukoulis, C.-T. Chan, and D. Turner, Phys. Rev. B **53**, 8340 (1996).
[21] E. D. Palik, *The Handbook of Optical Constants of Solids* (Academic, New York, 1993).
[22] G. Guida, D. Maystre, G. Tayeb, and P. Vincent, J. Opt. Soc. Am. B **15**, 2308 (1998).